Hindawi Publishing Corporation
Mathematical Problems in Engineering
Volume 2016, Article ID 4720867, 11 pages
http://dx.doi.org/10.1155/2016/4720867

Research Article

Analytical Analysis and Field Observation of Break Line in the Main Roof over the Goaf Edge of Longwall Coal Mines

Zhang Guangchao,[1] He Fulian,[1] and Jiang Lishuai[2]

[1]*College of Resources & Safety Engineering, China University of Mining & Technology (Beijing), Beijing 100083, China*
[2]*Shandong University of Science & Technology, Qingdao 266510, China*

Correspondence should be addressed to Zhang Guangchao; 874557858@qq.com

Received 9 May 2016; Revised 12 June 2016; Accepted 15 September 2016

Academic Editor: Marek Lefik

This paper presents an integrated approach for analytical analysis and field tests to estimate the break line in a main roof over the goaf edge. An analytical model which treated the main roof as a beam seating on the Winkler foundation and subjected to nonuniformity roof loading was established. Further analysis of the bending moment distribution of such a main roof beam was undertaken. Based on the geological conditions pertaining to a case study at Wangjialing coal mine, Shanxi Province, China, the break line in the main roof in a typical longwall panel was calculated in the rib-sides at a distance of 5.6 to 7.4 m from the goaf edge. The influence of main roof flexural rigidity and foundation rigidity and so forth on the bending moment distribution was revealed by a parametric study. Borehole camera detection was employed to further validate the analytical model and its results. The results of the field test demonstrated that the break line detected in the main roof was about 5.5 to 6.8 m away from the goaf edge, which was in good agreement with the analytical model.

1. Introduction

Entry driven along goaf edge (EDG) is a kind of gateroad, which is excavated as the tailgate or headgate for future panel by retaining a narrow coal pillar along the goaf edge of the previous panel [1]. The application of the EDG technique not only can increase coal recovery rate and achieve huge economic benefits but also can improve the drivage efficiency to shorten the time needed to prepare future panel [2]. Both generalised models and investigations show that, after excavation of the adjacent panel, a destressed zone and an overstressed zone are created in the rib-sides due to stress redistribution induced by the rotation and subsidence of the lateral main roof, and the two zones are demarcated by the break line, where the main roof is broken above the rib-sides [1, 3]. The low stress environment in the destressed zone benefits the excavation and maintenance of EDG and can prevent dynamic disasters due to high stress [2], such as floor heave and coal bumps. Therefore, it is of significance in theoretical research and engineering application to acquire the stress distribution in the rib-sides, especially the break line of the lateral main roof, for designing pillar width for EDG ground stability.

To date, considerable investigations have provided a comprehensive understanding with respect to the spatial structural characteristics of overlying strata near a goaf. For instance, Peng treated the main roof above the caved zone as a cantilever beam structure for determination of shield roof loading [4]. Smart and Davies presented a roof beam tilt theory, in which the inclination angle of the main roof strata and the rotation fulcrum position were considered as the important parameters for pillar width design [5]. However, both of the aforementioned analytical methods focus on the structural characteristics of broken roof strata, while how to obtain the break line in the main roof is often overlooked. Shi et al. proposed an analytical model for analysing the bending moment distribution along the main roof and found that the break line in the lateral main roof was just sited above the goaf edge [6]. In their model, the lateral main roof was simplified to be a cantilever beam fixed at a rigid abutment with zero vertical deflection. However, in reality, some investigations demonstrated that the break line in the lateral main roof was

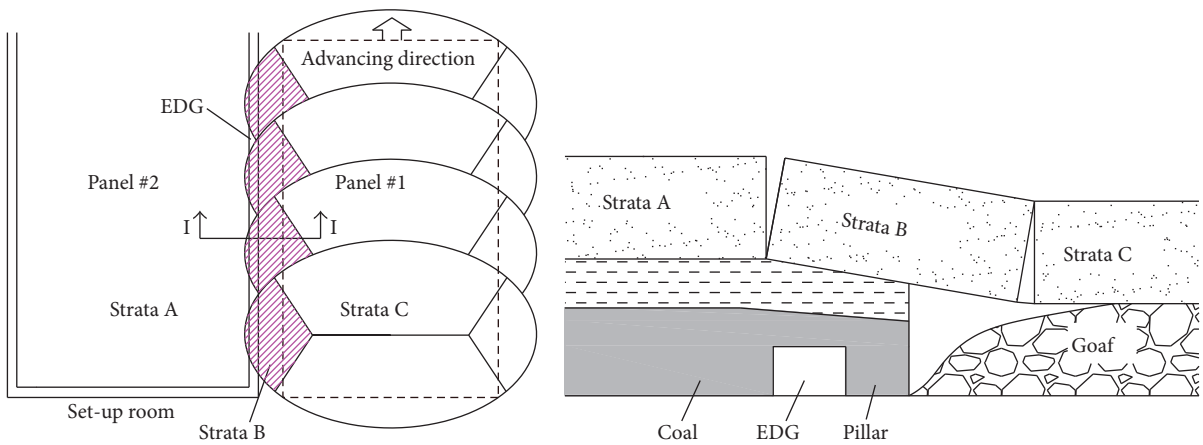

(a) Arc-triangle section of the lateral main roof after breakage (b) The lateral hinged structure over the EDG (section I-I in Figure 1(a))

Figure 1: Schematic arc-top structure above GDE.

usually several metres away from the goaf edge. For example, Zhang et al. performed physical experiments in which the lateral main roof broke at a distance of 3 to 8 m from the goaf edge and the break line moved closer to the goaf edge with immediate roof thickness decreasing [7]. Zhao and Qian established an elastic foundation beam model which treated the lateral main roof as an elastic beam resting on a Winkler medium [8]. Some results from their study demonstrated that the break line in the main roof lies in the rib-sides and varies with respect to the foundation rigidity. Unfortunately, the cover stress and side abutment pressure induced by adjacent panel mining were neglected in their model.

In addition, some scholars attempt to detect the break line in the lateral main roof by field studies. For instance, Wang et al. applied borehole stress meters to monitor the stress distribution in the rib-sides and got distributions of side abutment pressure [9]. Liu et al. presented experimental studies of strata movement above the goaf edge by seismic measurement techniques [10]. During the breakage process of the main roof, numerous vertical and subvertical fractures and horizontal cracks are sharply developed in the rock mass neighbouring the break line [4]. According to these characteristics, Zhang et al. presented an experimental research into the break line in the main roof by observing fractures evolution in a 10 m long borehole drilled on the GDE roof [11]. The results suggested that, compared to other monitoring methods, borehole camera detection was an effective, straightforward method to estimate the break line in the main roof.

In this paper, considering the deformation characteristics of coal seam, a simple analytical model was established to deduce the break line in the lateral main roof. Taking the case of panel 20105, Wangjialing coal mine, China, as an example, the influencing factors were investigated by a parametric study, such as Young's modulus, coal seam thickness, and foundation rigidity. The analytical solution was obtained and compared to a field study using borehole camera detection techniques for validation.

2. Mechanical Analysis

In longwall mining, when the work face advances a certain distance, the immediate roof collapses at first; then the main roof begins to bend and sag, causing crack generation and propagation in roof strata; once cracks coalesce into large fractures, the main roofs are broken into blocks. The broken strata hinge with adjacent strata and thus form an articulated structure above the coal face [12]. Meanwhile, perpendicular to the retreat direction of the work face, the lateral main roof shaped like arc-triangle section will be formed at the end of the mining panel, as shown in Figure 1(a). According to Bai [13], the lateral main roof will break in the rib-sides and then a lateral articulated structure is formed by broken strata A, B, and C, as illustrated in Figure 1(b). Investigations show that the structural characteristics of the lateral main roof, especially the break line thereof, will greatly affect the stress distribution in the rib-sides.

The section of lateral main roof before breakage is illustrated in Figure 2(a), where L is the length of the cantilever roof strata above the goaf and b is the extent of affected zone by side abutment pressure, which is about 40 to 60 m. Considering the fact that coal seams and their surrounding rock strata are relatively soft and weak compared to roof strata, they are considered to meet Winkler foundation assumptions [8, 14–16]. According to the available literature [15], the characteristic length of main roof is about 3.2 to 6.3 m, while the distribution area of side abutment pressure is about 40 to 60 m wide, which is about 5 to 20 times the characteristic length. Hence, the main roof above the rib-sides can be assumed to be a semi-infinite long beam on the Winkler foundation, and the main roof above the goaf is simplified to a cantilever supported by broken strata C, as shown in Figure 2(b). In Figure 2(b), M_0, Q_0, and N are the bending moment and shear and horizontal force acting at point $x = 0$; N' and Q' are the horizontal and shear force exerted by strata C, which act on the rear end of

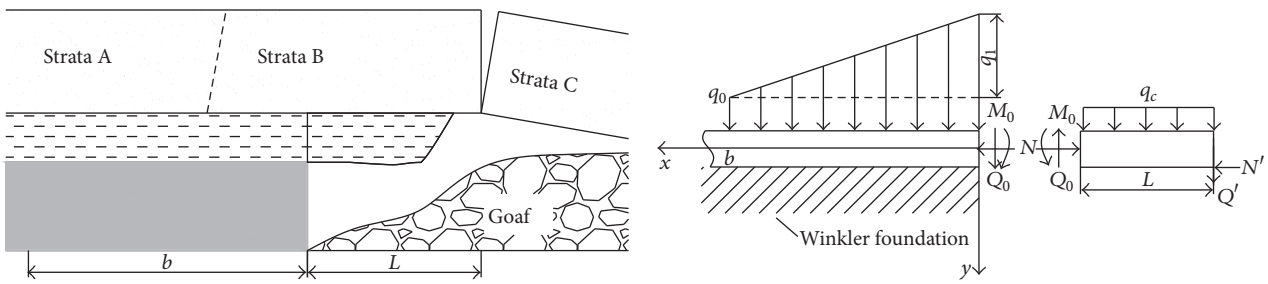

(a) Spatial structure (b) Analytical model layout

Figure 2: The main roof beam on a Winkler foundation.

the cantilever district. The roof beam atop the abutment is loaded by pressure $q(x)$, which consists of the overburden pressure q_0 and side abutment pressure. In this paper, the coal seam and its surrounding rock strata are assumed to be in perfectly elastic state; thus the location of the side abutment peak pressure is considered to be right above the work face wall. In practice, the location of the side abutment peak pressure varies with respect to the failure of coal, which is beyond the scope of the current study and will be further investigated in the future. Therefore, the side abutment pressure in this study is simplified to follow a linear relationship, which ranges from q_1 at $x = 0$ to 0 at $x = b$. The pressure $q(x)$ can be expressed by

$$q(x) = q_0 + \frac{b-x}{b} q_1, \tag{1}$$

where $q_0 = \gamma H$, $q_1 = k\gamma H$, γ is unit weight of overlying strata, H is the depth of panel below the ground face, and k is a stress increment coefficient, which is usually close to 1 [12]. The uniformly distributed load, q_c, shown in Figure 2(b), represents the overlying pressure on the cantilever district given by [12]:

$$q_c = \frac{E_1 h_1^3 (\gamma_1 h_1 + \gamma_2 h_2 + \cdots + \gamma_n h_n)}{E_1 h_1^3 + E_2 h_2^3 + \cdots + E_n h_n^3}, \tag{2}$$

where E_n is Young's modulus of nth layer above the panel, γ_n is unit weight of nth layer, and h_n is the thickness of nth layer.

According to Winkler's assumption [17], the relationship between pressure P and vertical deflection y of a foundation is given by

$$P = -Ky, \tag{3}$$

where P is the vertical stress acting on the beam due to the deflection of the foundation, y is the deflection of the foundation, and K is the stiffness modulus of the foundation, which is determined by the properties of rock strata below the main roof. Generally, the foundation can be considered as the combination of the immediate roof, coal seam, and immediate floor. Their interrelationship can be expressed as

$$\frac{1}{K} = \sum_1^m \frac{1}{K_m}, \qquad K_m = \frac{E_m}{(1-u_m^2) h_m}, \tag{4}$$

where K_m is the stiffness modulus of mth layer below the main roof; E_m, u_m, and h_m are Young's modulus, Poisson's ratio, and thickness of mth layer. According to the theory of beam bending on elastic foundation [18], the governing differential equation is

$$EI\frac{d^4 y}{dx^4} + N\frac{d^2 y}{dx^2} = q(x) + p, \tag{5}$$

where E is Young's modulus of the main roof, which, under plane strain conditions, is given by $E/(1-u^2)$; $I = dh^3/12$; d and h are the width and thickness of the main roof, respectively. Substituting (3) into (5) and assuming that $s = N/EI$ and $r^2 = K/EI$, the following equation can be given from (5):

$$\frac{d^4 y}{dx^4} + s\frac{d^2 y}{dx^2} + r^2 y = \frac{q(x)}{EI}. \tag{6}$$

According to the literature [12, 19], the general solution to homogeneous equation with respect to (6) is

$$Y(x) = e^{-\alpha x}(A\cos\beta x + B\sin\beta x), \tag{7}$$

where $\alpha = (r/2 - s/4)^{1/2}$ and $\beta = (r/2 + s/4)^{1/2}$. The particular solution to (6) is

$$Y^*(x) = \frac{q(x)}{EI\gamma^2}. \tag{8}$$

Thus, the general solution to (5) is

$$y(x) = e^{-\alpha x}(A\cos\beta x + B\sin\beta x) + \frac{q(x)}{EI\gamma^2}. \tag{9}$$

From Figure 2(b), the following relationships can be obtained at $x = 0$:

$$M_0 = EIy_0'',$$
$$Q_0 = EIy_0''' + Ny_0'. \tag{10}$$

Substituting (9) into (10), the roof beam deflection y is given by

$$y = e^{-\alpha x}\left[\left(\frac{\gamma M_0 + 2\alpha Q_0}{EI\gamma(\gamma - s)} + \frac{4\alpha q_1 s}{2kbr(r-s)}\right)\cos\beta x - \left(\frac{2\alpha\gamma M_0 + sQ_0}{2EI\gamma(\gamma - s)\beta} + \frac{q_1 s^2}{2kbr(r-s)\beta}\right)\sin\beta x\right]. \tag{11}$$

According to the bending moment expression $EIy'' = M(x)$, the bending moment M is given by

$$M = EIy'' = e^{-\alpha x}\left\{M_0\cos\beta x + \left[\frac{\alpha(\gamma + s)M_0 + \gamma Q_0}{(\gamma - s)\beta} + \frac{q_1 s}{br(r-s)\beta}\right]\sin\beta x\right\}. \tag{12}$$

The tensile stress in the main roof gradually increases with internal bending moment increasing; the main roof strata break off when the maximum tensile stress reaches its limited strength. Hence, the break line in the main roof can be obtained by calculating the location of the maximum bending moment. Take derivative to (12) and set $M' = 0$; the location of maximum bending moment x_0 can be obtained as follows:

$$\tan\beta x_0 = \frac{[(3as - ar)M_0 + \gamma Q_0 + q_1 s/br]\,2\beta}{(2\gamma^2 - s^2 + 2\gamma\beta^2 - 2s\beta^2)M_0 + 2\alpha\gamma Q_0 + 2asq_1/br},$$
$$x_0 = \frac{\tan^{-1}\left([(3as - ar)M_0 + \gamma Q_0 + q_1 s/br]\,\beta/\left(\left(\gamma^2 + \gamma\beta^2 - s\beta^2\right)M_0 + \alpha\gamma Q_0 + asq_1/br\right)\right)}{\beta}. \tag{13}$$

According to the equilibrium conditions and a voussoir beam theory [13], Q_0, M_0, Q', and N are given as follows:

$$Q_0 = q_c L + Q',$$
$$M_0 = \frac{1}{2}q_c L^2 + Q'L + N'\left(\frac{h}{2} + \Delta s_1\right),$$
$$N = \frac{LQ'}{2(h - \Delta s)},$$
$$Q' = L\gamma h, \tag{14}$$

where $\Delta s = h/6$; Δs is the deflection of broken strata. Δs_1 is the deflection of the rear end of cantilever roof strata relative to the position, where $x = 0$, which can be neglected due to its small value.

3. Case Study

3.1. Background of Wangjialing Coal Mine. To demonstrate the theoretical results, a case study was conducted in Wangjialing coal mine, Shanxi Province, China. The mining area of the Wangjialing coal mine is 7.0 km long and 25.8 km wide and covers a total of mining area of 180.6 km^2. Longwall panels 20103 and 20105 were selected for this case study. The two panels were 260 m wide in the strike direction and 1400 m long in the dip direction, serving for number 2 coal seam. Number 2 coal seam was buried at a depth of 300 m with an average thickness of 6.2 m. The immediate roof is sandy mudstone with an average thickness of 2.0 m. The main roof is siltstone with an average thickness of 9.2 m. The immediate floor is mudstone with an average thickness of 1.6 m. The density, Young's modulus, Poisson's ratio, uniaxial compressive strength (UCS), cohesion, and friction angle were measured by laboratory testing of samples cored from Wangjialing coal mine, as presented in Table 1. All of rock/coal properties were based on laboratory tests on coal and rock samples reported by North China Institute of Science and Technology [20]. Mechanical property laboratory tests of rock core samples of the coal seam have been conducted on a servo-controlled, special testing system (TAW-2000) having a maximum axial load of 2000 kN, maximum shear load of 500 kN, and maximum lateral pressure of 500 kN. It is noticed that the friction angle of coal is approximately the same as sandstone, while the cohesion and UCS of the coal are far smaller compared to sandstone. Without any evidence to suggest that the test results were erroneous, this value was used in the study.

After panel 20105 had been mined out, number 20103 headgate was developed along the goaf edge for panel 20103, as shown in Figure 3. The pillar between adjacent panels was 8 m wide.

3.2. Determination of Model Parameters. Based on the data in Table 1, RocLab software was used to determine the rock mass strength parameters. Related parameters are listed in Table 2, where GSI, M_i, and D are the geological strength index, the intact parameters, and disturbance factor, respectively. UCS and E_i are the uniaxial compression strength and Young's modulus of intact rock, respectively, and E_{rm} is Young's modulus of the rock mass.

3.3. Bending Moment Distribution. According to (4) and the mechanical properties of the immediate roof, coal seam,

Table 1: Generalised stratigraphy and key geotechnical parameters.

Stratum number	Geological legend	Rock type	Rock thickness (m)			Density (kg/m^3)	Young's modulus (GPa)	Poisson's ratio	UCS (MPa)	Cohesion (MPa)	Friction angle (°)
			Maximum	Minimum	Average						
1		Fine sandstone	4.9	6.22	5.6	2700	27.73	0.22	165.3	11.6	41.64
2		Mudstone	1.49	2.12	1.8	2140	6.85	0.24	44.6	2.6	32
3		Fine sandstone	0.2	1.52	0.9	2700	27.73	0.22	165.3	11.6	41.64
4		Mudstone	0.9	1.58	1.3	2140	6.85	0.24	44.6	2.6	32
5		Medium sandstone	1.89	2.56	2.3	2675	28.14	0.21	146.2	10.9	47.64
6		Gritstone	1.4	2.2	1.7	2730	32.66	0.24	162.4	12.4	48.23
7		Coal seam	0.9	1.2	1.0	1412	2.06	0.36	13.89	2.3	44.34
8		Mudstone	2.1	3.2	2.3	2140	6.85	0.24	44.6	2.6	32
9		Siltstone	8.9	12.6	9.2	2680	30.73	0.22	142.3	9.4	39.42
10		Sandy mudstone	1.66	2.3	2.0	2659	11.58	0.27	63.28	8.9	47.39
11		Coal seam #2	5.96	6.6	6.2	1412	2.06	0.36	13.89	2.3	44.34
12		Mudstone	1.4	1.8	1.6	2140	6.85	0.24	44.6	2.6	32
13		Siltstone	5.9	7.7	6.8	2680	30.73	0.22	142.3	9.4	39.42

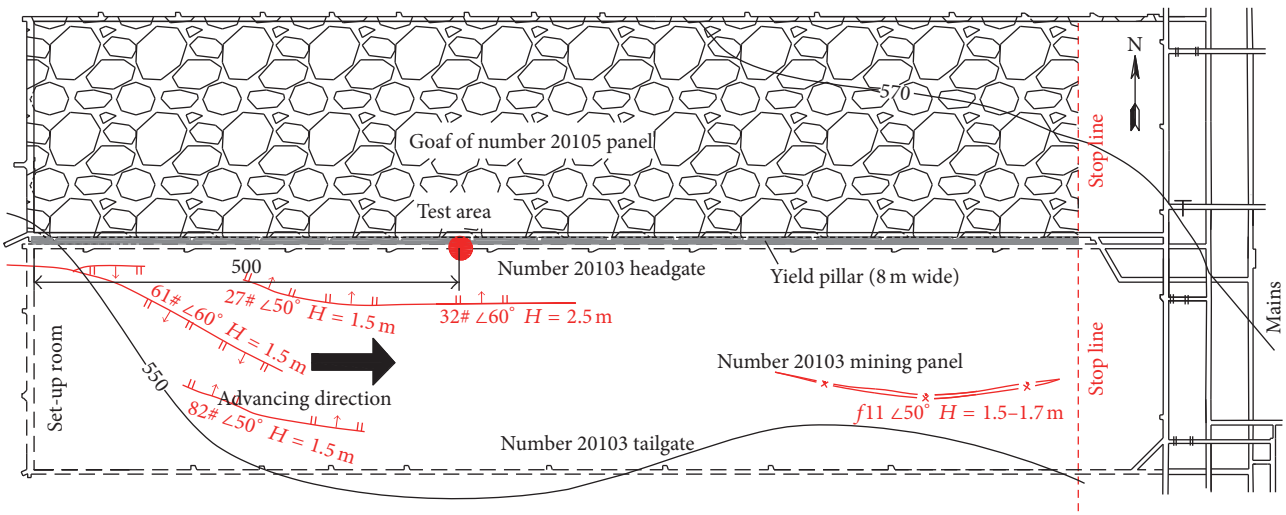

Figure 3: Layout of panels 20105 and 20103 and location of test area in number 20103 headgate.

Table 2: Properties of coal and roof formation.

Lithology	UCS/(MPa)	GSI	M_i	D	E_i/(GPa)	E_{rm}/(GPa)
Fine sandstone	165.3	64	14	0.7	27.73	14.55
Medium sandstone	146.2	66	16	0.7	28.14	16.327
Gritstone	162.4	72	17	0.7	32.66	23.06
Siltstone	142.3	70	16	0.7	30.73	20.55
Sandy mudstone	63.28	43	11	0.7	11.58	3.46
Coal seam	13.89	14	4	0.7	2.06	0.30
Mudstone	44.6	47	9	0.7	6.85	3.65

and floor in Table 2, the stiffness modulus of foundation K is calculated to be 0.06 GPa.

Based on the key stratum theory, strata number 2 to number 9 will deflect with the main roof strata. Using (2) and the data from Table 2, cantilever district roof beam load intensity $q_c = 0.50$ MPa.

Young's modulus of main roof is calculated to be 21.59 GPa, the moment of inertia I is 64.89 m^4, and thus the flexural rigidity is 1400.98 GN·m^2.

The length of cantilever is consistent with the periodic weighting length, which is 14 m. We have the following:

$$Q' = 14\,\text{m} \times (25\,\text{KN/m}^2 \times 9.2\,\text{m}) = 3.22\,\text{MN}.$$

$$N = 14\,\text{m} \times 3.22\,\text{MN}/(5 \times 9.2\,\text{m}/3) = 2.94\,\text{MN}.$$

$$Q_0 = 0.50\,\text{MN/m} \times 14\,\text{m} + 3.22\,\text{MN} = 10.22\,\text{MN}.$$

$$M = 0.50\,\text{MN/m} \times 14\,\text{m} \times 14\,\text{m}/2 + 3.22\,\text{MN} \times 14\,\text{m} + 2.94\,\text{MN} \times 4.6\,\text{m} = 107.60\,\text{MN} \cdot \text{m}.$$

Then, $\gamma = 0.007\,\text{m}^{-2}$ and $s = 2.099 \times 10^{-6}\,\text{m}^{-2}$.

Substituting parameters into (11) and (12), the deflection and bending moment in the main roof can be obtained as shown in Figure 4 and Table 3.

The distribution of bending moment in the main roof is shown in Figure 4. The bending moment increases from the goaf edge and hit the peak at a distance of 6 to 7 m away from the goaf edge, and then it decreases to zero in distance

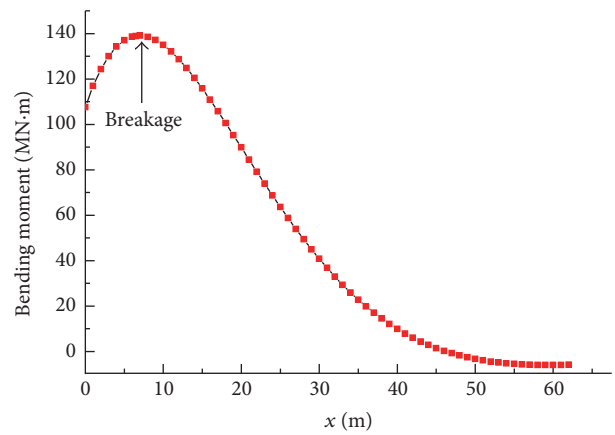

Figure 4: Distribution of bending moment along beam.

from goaf edge within 60 m. This differs from traditional models employing the assumption of rigid abutment in that the maximum bending moment occurs in the rib-sides rather than just above the goaf edge. It highlights the benefit of the present model treating the coal seam abutment as an elastic foundation. The bending moment is greater than 139 MN·m at a distance of 5.6 to 7.4 m from the goaf edge, yet it is lower than 139 MN elsewhere as shown in Table 3. It can therefore be concluded that the break line in the main roof is located at a distance of 5.6 to 7.4 m from the goaf edge.

4. Model Parametric Study

4.1. Effect of Foundation Rigidity. The effect of foundation rigidity on the bending moment distribution along main roof is shown in Figure 5. Figure 6 shows the magnitude and location of the maximum bending moment for different foundation rigidities. As the foundation rigidity increases from 0.025 GPa to 1 GPa, the maximum bending moment decreases linearly from 153.6 MN·m to 118.6 MN·m; the location of the maximum bending moment moves from 10.3 m

Table 3: Variation of bending moment and deflection along the beam.

x/m	0	1	2	3	4	5	6	7	8	10	12	15	20	25	30	40	50
Bending moment (MN·m)	107	117	124	130	134	137	139	139	138	135	128	115	89	63	40	9.8	3.3

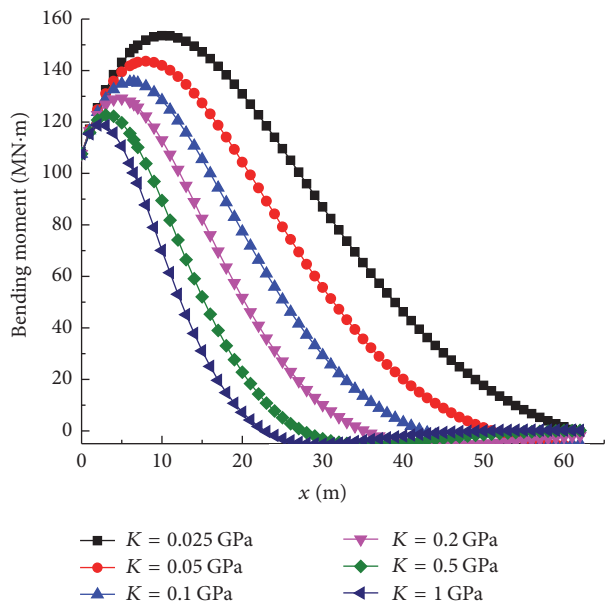

Figure 5: Bending moment distribution along the main roof for different foundation rigidities.

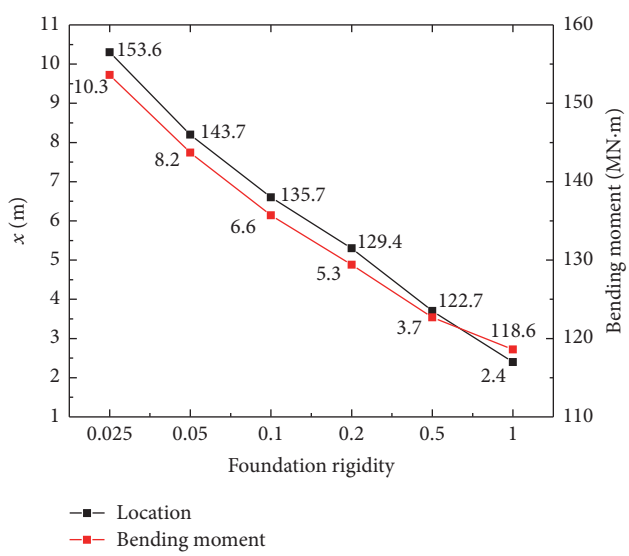

Figure 6: Relationship between bending moment and foundation rigidity.

from the goaf edge to 2.4 m from it. These results suggest that the foundation rigidity has a pronounced effect on the beam bending moment distribution.

According to (4), the modulus of foundation rigidity is seriously affected by the mechanical properties and thickness of the coal seam. Hence, the break line in the main roof can be greatly influenced by the foundation rigidity, that is, the rigidity of the coal seam, which is of great significance in determination of the location of EDG.

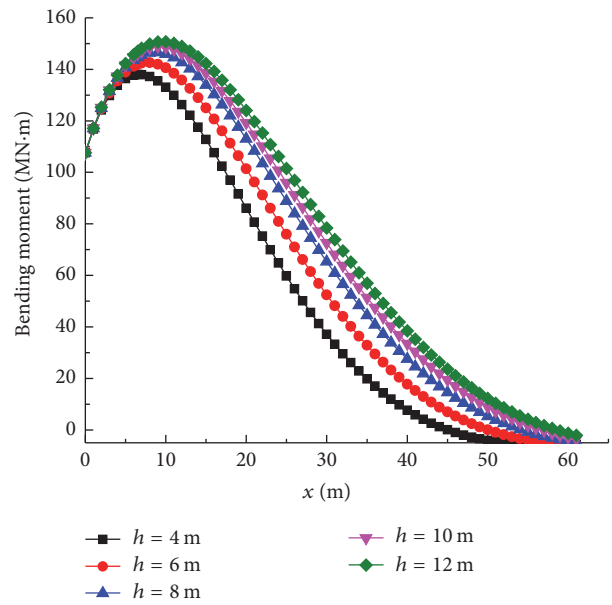

Figure 7: Bending moment distribution along the main roof for different coal seam thicknesses.

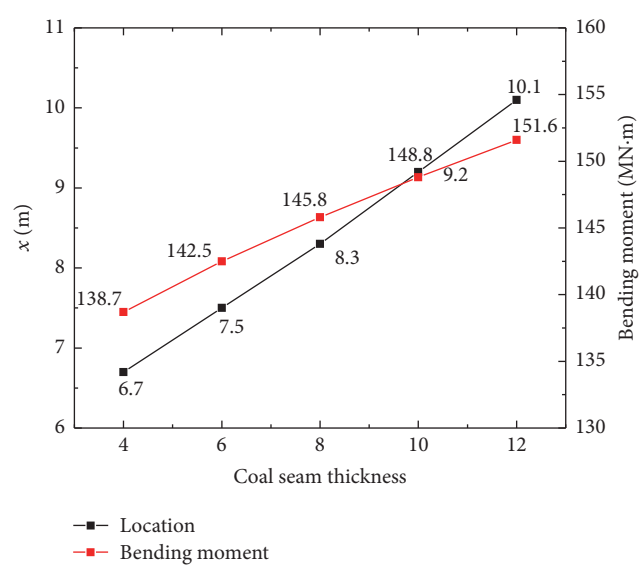

Figure 8: Relationship between bending moment and coal seam thickness.

4.2. Effect of Coal Seam Thickness. Figure 7 shows the effect of coal seam thickness on the bending moment distribution along the main roof. Figure 8 shows the magnitude and location of the maximum bending moment for different coal seam thickness. As the coal seam thickness increases, the maximum bending moment increases from 138.7 MN·m to 151.6 MN·m; the location of the maximum bending moment moves from 6.7 m to 10.1 m. These changes can be attributed

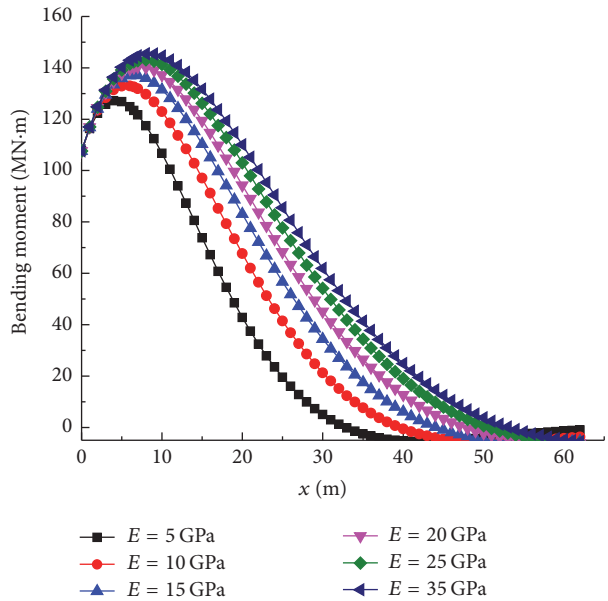

Figure 9: Bending moment distribution along the main roof for different Young's modulus of main roof.

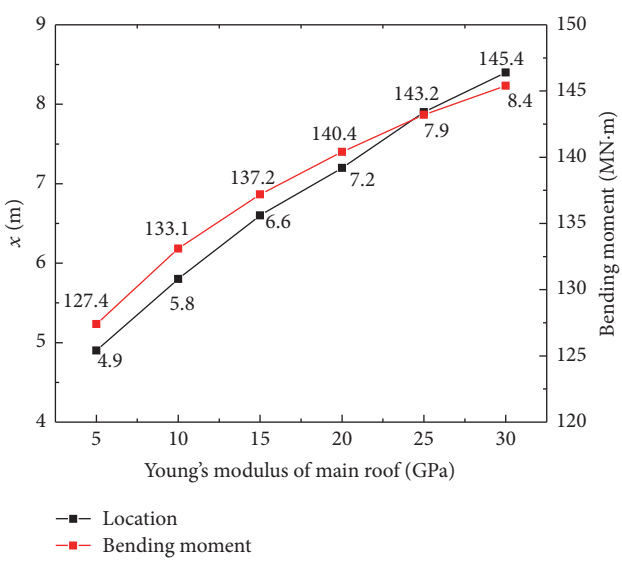

Figure 10: Relationship between bending moment and Young's modulus of main roof.

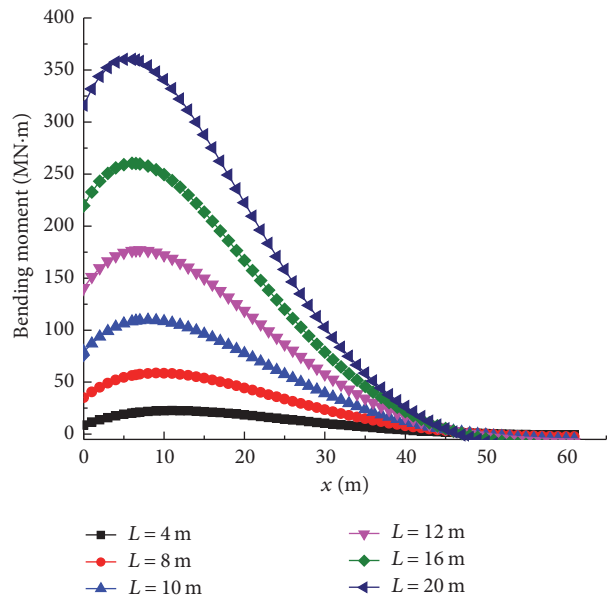

Figure 11: Bending moment distribution along the main roof with different cantilever roof lengths.

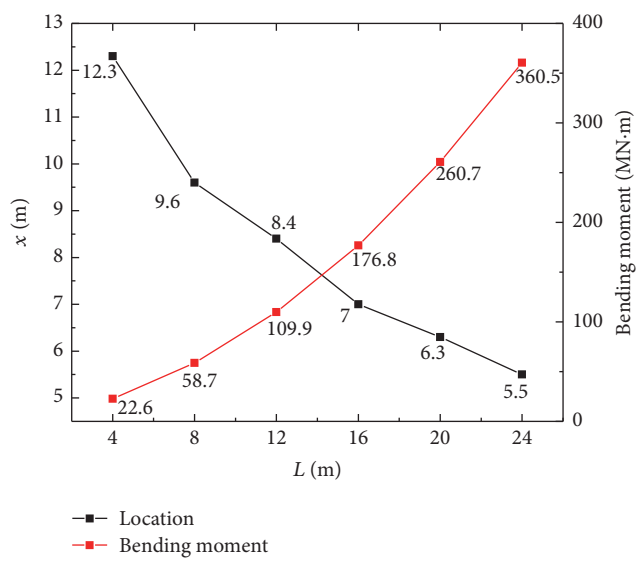

Figure 12: Relationship between bending moment and foundation rigidity.

to the reduced foundation rigidity, as coal seam thickness increases (see (4)). Similarly, according to (4), the thickness of the immediate roof or floor strata has the same effect on the bending moment distribution along the main roof.

4.3. Effect of Main Roof Flexural Rigidity. The bending moment distribution along main roof for different roof's Young's modulus is shown in Figure 9. The magnitude and location of the maximum bending moment also vary with Young's modulus, as illustrated in Figure 10. As the roof's Young's modulus increases from 5 GPa to 30 GPa, the maximum bending moment increases from 127.4 MN·m to 145.4 MN·m, and the location of maximum bending moment moves from 4.9 m to 8.4 m. The results suggest that a variation in main roof rigidity has a significant effect on the break line in the main roof and thereby explains the high side abutment pressure concentration region over 60 m deep into the goaf edge on the conditions that the main roof is with thick and hard strata [21].

4.4. Effect of Cantilever Roof Length. The bending moment along the main roof is directly influenced by the length of the cantilever roof. Figure 11 shows the bending moment distribution along the main roof for different cantilever roof lengths. As can be seen, significant bending moment profile difference along roof beam can be noticed with a small increase of cantilever roof length. Figure 12 shows

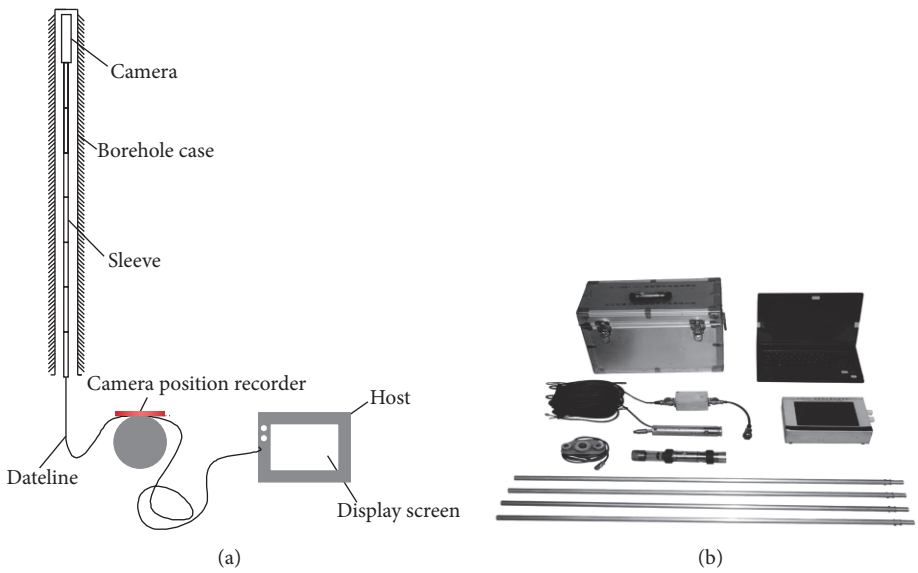

Figure 13: Schematic of the YSZ(B) panoramic borehole camera system. (a) Digital panoramic borehole camera system composed of a camera, sleeve, a camera position recorder, dateline, and a host. (b) Test equipment.

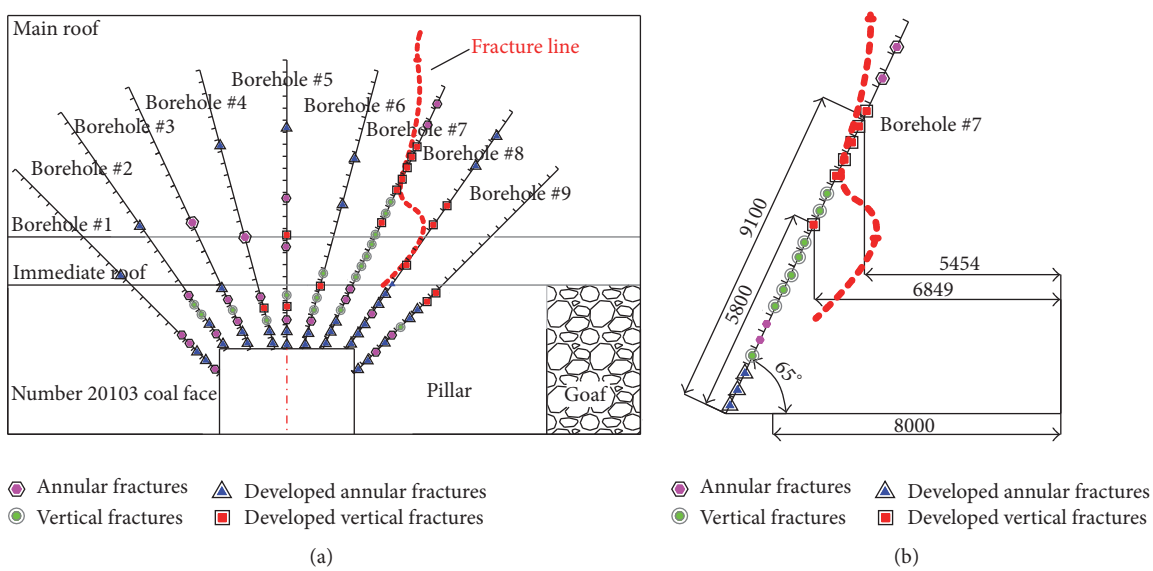

Figure 14: Detected roof fracture zones: (a) detected roof fracture zones and (b) determination of fracture line location.

the relationship between maximum bending moment and cantilever roof length. As cantilever length increases from 4 to 24 m, the maximum bending moment increases from 22.6 MN·m to 360.5 MN·m, while the location of maximum bending moment moves from 12.3 m to 5.5 m. As expected, the length of cantilever roof plays an important role in the broken behaviour of the main roof.

5. Field Tests and Discussion

5.1. Borehole Camera Detection. To validate the analytical model, borehole camera detection was employed to detect the break line in the main roof. As shown in Figure 13, YSZ(B) panoramic borehole camera system consists of a camera, sleeves, data lines, a camera position recorder, and a host. The corresponding borehole with which it works is 28 mm in diameter. During observation, the video or image down the borehole can be recorded and transmitted to the host in real time. And then we can acquire the break line in the main roof by observing the crack propagation in rock masses.

5.2. Analysis of Borehole Camera Detection Data. A section along number 20103 headgate and 500 m from the set-up room was selected as a test area to assess the break line in the main roof, as shown in Figure 3. The arrangement of boreholes and the distribution of fractures along borehole are illustrated in Figure 14.

As shown from the images of borehole #2, annular fractures were well developed at a depth of 0 to 1.5 m down the borehole; rock was almost intact at a depth of

1.5 to 2.0 m with some tiny annular or vertical fractures. In the depth of 2.5 m and beyond, the rock mass was intact. For borehole #4, annular fractures were developed at a depth of 0 to 1.2 m. Only some tiny vertical fractures were observed at a depth of 1.2 to 2.0 m. At 2.0 m and beyond, the rock was intact. For borehole #7, the fracture densities in the borehole increased compared with boreholes #2 and #4. Both annular and vertical fractures were observed in the region of 0 to 3.0 m down the borehole. At a depth of 3.0 to 4.9 m, the fractures densities decreased slightly. At 4.9 m and beyond, vertical fractures became well developed even throughout the borehole resulting in serious damage and collapse at a depth of 7.2 to 8.9 m. The rock remained intact beyond 10 m. As seen in borehole #8, annular fractures and tiny vertical fractures were observed at a depth of 0 to 3.8 m along the borehole. Vertical fractures were well developed at a depth of 4.4 to 7.6 m. No fractures were observed beyond a depth of 7.6 m.

Based on the above analysis, fractures in rock masses can be classified into four types, namely, annular, vertical, developed annular, and developed vertical fractures. The following, therefore, can be concluded.

(1) The damaged zone in boreholes #1 to #6 was about 1.2 to 2.5 m, while the damaged zone in boreholes #7 to #8 developed to the main roof strata. In addition, the asymmetric deformation was also observed *in situ*; severe squeezing failure and step convergence occurred at the roof of pillar side, while the roof of solid coal side remained intact mainly. This asymmetric failure was due to the asymmetric distributed side abutment pressure along the roof beam induced by main roof breakage.

(2) The top-slice coal was severely damaged with developed annular fractures and rock separation. The reason was that the top-slice coal was with lower strength than siltstone and sandy mudstone, which was easily failed affected by the dynamic pressure exerted by the adjacent panel mining and headgate development.

(3) Compared with roof of solid coal side, vertical fractures were well developed in the deep of main roof above the coal pillar. These highly developed vertical fractures indicated that the break line in main roof was more likely located above the coal pillar. That is, because rock mass is a weaker material with low tensile strength, numerous vertical and subvertical fractures developed in rock masses during the process of main roof breakage.

(4) The images of borehole #7 revealed that the vertical fractures developed throughout the borehole and formed a crushed zone at a depth of 5.8 to 9.1 m down the borehole, as shown in Figure 14(a). According to the length and inclination angle of borehole #7, it can then be deduced that the crushed zone was at a distance of 5.454 to 6.847 m from the goaf edge; in other words, the break line in the main roof is 5.5 to 6.8 m away from the goaf edge as presented in Figure 14(b).

Based on the analysis above, the break line in the main roof detected *in situ* is in good agreement with the analytical model, which implies that the model is capable of an assessment of the break line in the lateral main roof. The research provides a simple and reliable analytical method to estimate the break line in the lateral main roof, which will be significant when designing the pillar width for a safe, stable, EDG condition.

6. Conclusion

Accurately acquiring the break line in main roof is of great importance in pillar width design and EDG maintenance. In this research, the break line was acquired through an integrated method combining theoretical analysis and field tests. By comparison with previous studies, this work contained the following original aspects. (1) The spatial model which treated the lateral main roof as a beam supported by a Winkler foundation and subjected to nonuniform loading was proposed. The break line in the main roof can be obtained by calculating the maximum bending moment along the roof beam. (2) The break line in the main roof was influenced by the foundation rigidity, Young's modulus of the main roof and coal seams, and the length of the cantilever roof. (3) Many vertical and subvertical fractures sharply developed in rock masses during the process of main roof breakage. Thus, the break line in the main roof can be detected by observing the fractures distribution in the roof strata.

Field tests conducted in number 20103 headgate, Wangjialing coalmine, Shanxi Province, demonstrated that the break line in the main roof detected *in situ* was in good agreement with the analytical analysis, which verified the validity of the analytical model.

It should be noted that the side abutment pressure was simplified to a triangular distribution and the peak side abutment pressure was located at the goaf edge. Further research was deemed necessary to perfect the distribution of side abutment stress to improve the model. In addition, more field tests should be conducted to validate the model.

Competing Interests

The authors declare that they have no competing interests.

Acknowledgments

This work was supported by National Natural Science Foundation of China under Grant 51574243 and the Fundamental Research Funds for the Central Universities under Grant 2010YZ02.

References

[1] S. Yan, J. Bai, X. Wang, and L. Huo, "An innovative approach for gateroad layout in highly gassy longwall top coal caving," *International Journal of Rock Mechanics and Mining Sciences*, vol. 59, pp. 33–41, 2013.

[2] W. Li, J. Bai, S. Peng, X. Wang, and Y. Xu, "Numerical modeling for yield pillar design: a case study," *Rock Mechanics and Rock Engineering*, vol. 48, no. 1, pp. 305–318, 2015.

[3] H. Yavuz, "An estimation method for cover pressure re-establishment distance and pressure distribution in the goaf of longwall coal mines," *International Journal of Rock Mechanics and Mining Sciences*, vol. 41, no. 2, pp. 193–205, 2004.

[4] S. Peng, *Coal Mine Ground Control*, Department of Mining Engineering/College of Engineering and Mineral Resources, Morgantown, WVa, USA, 2008.

[5] B. Smart and D. Davies, "Application of the rock-strata-title approach to the pack design in an arch-sharped roadway," *Minerals Engineering*, vol. 144, no. 9, pp. 91–178, 1982.

[6] J. J. Shi, N. J. Ma, and Z. S. Bai, "Analysis on roof broken location of gateway retained along goaf and technology of roof support," *Coal Science and Technology*, vol. 41, no. 7, pp. 35–42, 2013.

[7] N. Zhang, L. Yuan, C. Han, J. Xue, and J. Kan, "Stability and deformation of surrounding rock in pillarless gob-side entry retaining," *Safety Science*, vol. 50, no. 4, pp. 593–599, 2012.

[8] G. J. Zhao and M. G. Qian, "The behaviour of the main roof fracture in longwall mining and its effect on roof pressure," in *Proceedings of the 28th US Symposium on Rock Mechanics*, pp. 1–8, Tucson, Ariz, USA, June-July 1987.

[9] D. Wang, S. Li, Q. Wang et al., "Experimental study of reasonable coal pillar width in fully mechanized top coal caving face of deep thick coal seam," *Chinese Journal of Rock Mechanics and Engineering*, vol. 33, no. 3, pp. 539–548, 2014.

[10] J. H. Liu, F. X. Jiang, N. G. Wang, Z. S. Li, and Z. G. Zhang, "Research on reasonable width of segment pillar of fully mechanized caving face in extra-thick coal seam of deep shaft," *Chinese Journal of Rock Mechanics and Engineering*, vol. 31, no. 5, pp. 921–927, 2012.

[11] Y. Zhang, Z.-J. Wan, F.-C. Li et al., "Large deformation mechanism of roadway driving along goaf under unstable overlying rock strata," *Journal of Mining and Safety Engineering*, vol. 29, no. 4, pp. 451–458, 2012.

[12] M. G. Qian and P. W. Shi, *Mining Pressure and Strata Control*, China University of Mining and Technology Press, Xuzhou, China, 2003.

[13] J. Bai, *Surrounding Rock Control of Gob-Side Entry Driving*, China University of Mining and Technology Press, Xuzhou, China, 2006.

[14] J. Q. Jiang, *Surrounding Rock Stress and Movement in Stope*, China Coal Industry Publishing House, Beijing, China, 1993.

[15] X. Li, N. Ma, Y. Zhong, and Q. Gao, "Storage and release regular of elastic energy distribution in tight roof fracturing," *Chinese Journal of Rock Mechanics and Engineering*, vol. 26, no. 1, pp. 2786–2793, 2007.

[16] L. Jiang, H. S. Mitri, N. Ma, and X. Zhao, "Effect of foundation rigidity on stratified roadway roof stability in underground coal mines," *Arabian Journal of Geosciences*, vol. 9, no. 1, pp. 1–12, 2016.

[17] E. Winkler, *Die Lehre yon der Elastizitat und Festigkeit*, H. Dominicus, Prague, Czech Republic, 1867.

[18] M. Hetényi, *Beams on Elastic Foundation: Theory with Applications in the Fields of Civil and Mechanical Engineering*, The University of Michigan Press, Ann Arbor, Mich, USA, 1971.

[19] S. Timoshenko, *Mechanics of Materials*, Science Press, Beijing, China, 1979.

[20] G. C. Zhang and F. L. He, "Asymmetric failure mechanism and control countermeasures of large cross-section gob-side entry roof with fully-mechanized caving mining," *Chinese Journal of Rock Mechanics and Engineering*, vol. 35, pp. 806–817, 2016.

[21] B. Yu, C. Y. Liu, and L. J. Rong, "Mechanism and control technology of pressure occurrence in roadway with extra thickness and mechanized caving coal seam in Datong mining area," *Chinese Journal of Rock Mechanics and Engineering*, vol. 33, pp. 1863–1872, 2014.